Unique Rheological Behavior of Chitosan-Modified Nanoclay at Highly Hydrated State

ARTICLE *in* THE JOURNAL OF PHYSICAL CHEMISTRY B · APRIL 2009

Impact Factor: 3.3 · DOI: 10.1021/jp8107304 · Source: PubMed

Unique Rheological Behavior of Chitosan-Modified Nanoclay at Highly Hydrated State

Songmiao Liang,[†] Linshu Liu,[‡] Qingrong Huang,[†] and Kit L. Yam*,[†]

Department of Food Science, Rutgers University, 65 Dudley Road, New Brunswick, New Jersey 08901, Eastern Regional Research Center, United States Department of Agriculture, 600 East Mermaid Lane, Wyndmoor, Pennsylvania 19038

Received: December 6, 2008; Revised Manuscript Received: March 10, 2009

This work attempts to explore the dynamic and steady-state rheological properties of chitosan modified clay (CMCs) at highly hydrated state. CMCs with different initial chitosan/clay weight ratios (*s*) were prepared from pre-exfoliated clay via electrostatic adsorption process. Thermogravimetric analysis and optical microscopy were used to determine the adsorbed content of chitosan (*m*) in CMCs and the microstructure of CMCs at highly hydrated state, respectively. Dynamic rheological results indicate that both stress−strain behavior and moduli of CMCs exhibit strong dependence on *m*. Shear-thinning behavior for all of CMCs is observed and further confirmed by steady-state shear test. Interestingly, two unique transitions, denoted as a small peak region of the shear viscosity for CMCs with $m > 2.1\%$ and a sharp drop region of the shear viscosity for CMCs with $m \leq 6.3\%$, were observed at shear rate range of about $10 < \dot{\gamma} < 40$ and $0.2 < \dot{\gamma} < 0.5$ s^{-1}, respectively. Further, analysis on the recovery of CMCs at rest after underwent a preshearing process was performed with an emphasis to explain the presence of these unique transitions. Thixotropic effect was observed in CMCs and showed strong dependence on *m* and the preshearing history. Failure to Cox−Merz rule of the rheological behavior of CMCs suggests that some preferential orientation of the initial quiescent random arrangement of CMCs particles or their tactoids occurs under the applied shearing.

Introduction

Silicate clay has been extensively applied for developing high performance materials due to its unique combination of mechanical and thermal properties.[1−7] It is composed of individual microscopic sheets and has a highly layered sandwichlike structure. Each sheet has a thickness of about 1 nm and lateral dimension between 100 to 1000 nm.[8,9] Excess negative charges usually exists on the surface of each sheet since a part of Al^{3+} and Si^{4+} in aluminum−oxygen octahedron and silicon−oxygen tetrahedron of clay crystal cell were replaced by Mg^{2+}. As a matter of fact, hydrated sodium ions and other ions were adsorbed in the gallery space between the sheets through electrostatic adsorption to keep an electrostatic balance. These hydrated ions have the ability easily to exchange with other organic and inorganic ions through cationic exchange process.[10−12] The ion exchange capability of silicate clay has been determined at about 0.9∼1.2 mequiv/g.[10,11] It has been reported that modification of clay with organic cations cannot only effectively decrease its surface tension but promote its compatibility with polymer substrate and monomers.[13−15] More important, this kind of modification on clay provides an essential way to introduce different functional groups so that design materials with required structure and performance.[16−19]

One of the most fantastic examples is the interaction between clay and biopolymers such as proteins[20] and polysaccharides.[21−24] Because of the polycationic nature of chitosan in acidic media, it has been reported that chitosan could intercalate into pristine clay to form chitosan/clay nanocomposites (CCNs) by means of cationic exchange process.[25−28] Strong electrostatic interaction between chitosan and clay was observed to exist in these systems. Bilayered structure of chitosan has been built in the gallery space during the CCNs preparation process. The first layer took place mainly through electrostatic interaction between the NH_3^+ groups of chitosan and the negative sites on the surface of the clay platelets while the second layer was established by hydrogen bonding interaction between amino and hydroxyl groups in the chitosan chain.[28] This special arrangement of chitosan in clay allows such a CCN to possibly act as a sensor to potentiometrically determine some anions, especially monovalent anions.[28] Moreover, enhanced mechanical properties and thermal stability of CCNs have been reported as a result of the strong clay-chitosan interaction[27] and the synergistic effect between two-dimensional (2D) clay platelets and 1D carbon nanotubes (CNTs) in CCNs.[29]

However, although much work has been focused on the structure and properties of chitosan modified clay (CMC) or CCNs, rheological behavior of these hybrid materials at molten state and especially at highly hydrated state has not been systematically addressed yet. Compared to those previously developed nanocomposites,[30−37] CMCs could have some unique rheological behaviors because of the semiflexible chain conformation of chitosan and its strong electrostatic interaction with clay. In the present work, highly hydrated CMCs with different adsorbed content of chitosan were prepared from electrostatic adsorption process. The clay used here was pre-exfoliated by strong mechanical shearing process to get adequate dispersion. Similar treatments have been used to prepare nanoclay-reinforced hydrogels, which have associative network and excellent mechanical performance.[38−40] The adsorbed content of chitosan and the microstructure of CMCs at highly hydrated state were determined by thermogravimetric analysis (TG) and optical microscopy, respectively. As the main subject of this work, rheological behaviors of CMCs at a highly hydrated state were studied by oscillatory shear and steady-state shear mea-

* To whom correspondence should be addressed. E-mail: yam@aesop.rutgers.edu.
[†] Rutgers University.
[‡] United States Department of Agriculture.

10.1021/jp8107304 CCC: $40.75
Published on Web 04/03/2009

surements. Effect of the adsorbed chitosan on their recovery at rest after underwent steady shear was further studied by dynamic time sweep. Our results clarified that both microstructure and rheological behavior of the highly hydrated CMCs are closely related to the adsorbed content of chitosan.

Experimental Section

Materials. Chitosan samples with deacetylation degree of 98% and molecular weight (M_w) of 330 KD were purchased from Kunpoong Bio. Co., LTD (South Korea). Silicate clay (Cloisite Na^+) was purchased from Southern Clay Products, Inc. All of these reagents were used as received. Milli-Q (18.3 MΩ) water was used in all experiments.

Sample Preparation. Two wt % chitosan solutions were obtained by dissolving 4 g chitosan powder in 196 g of 1 wt % acetic acid solution at room temperature. To prepare a suspension of pre-exfoliated clay, 5 g Cloisite Na^+ was dispersed in 495 g distilled water by a magnetic stirrer (Thermix Stirring Hot Plate Model 210T, Fisher Scientific) at 1500 rpm for 48 h. The resultant solution was centrifuged at 3000 rpm for 30 min to remove larger particles. The final concentration of the pre-exfoliated clay in the semitransparent suspension is 0.92 wt %.

CMCs were prepared from solution mixing method at room temperature. In this method, 0.5, 1, 1.5, 2, 2.5, 3, 4, and 5 g of 2 wt % chitosan solutions were first adjusted to the same weight of 5 g using 1 wt % acetic acid solution, which will enable adsorption of chitosan on the clay surface to occur at the same conditions. Then, the adjusted chitosan solutions were separately injected into 20 g 0.92 wt % clay suspensions dropwise under a magnetic stirring of 200 rpm. In all of the cases, the resultant mixtures were kept stirring at 200 rpm for 1 h to establish adsorption equilibrium. The initial chitosan/clay weight ratios ($s = W_{Chitosan}/W_{Clay}$) in the chitosan/clay mixtures were correspondingly calculated as 0.06:1, 0.11:1, 0.16:1, 0.22:1, 0.27:1, 0.32:1, 0.44:1, and 0.56:1, respectively. After that, the CMCs slurries prepared from the above initial weight ratios were obtained by a centrifugation of 3000 rpm for 10 min. All of them were washed with pure water until free from acetate and were then sealed in centrifuge tubes for the next experiments. The water content in these CMCs slurries was measured as 97.3 ± 1.4 wt %. Concisely, the CMCs prepared here were denoted as CMCs-x, where $x = 6$, 11, 16, 22, 27, 32, 44, and 56 are corresponding to the initial chitosan/clay weight ratios $s = 0.06$:1, 0.11:1, 0.16:1, 0.22:1, 0.27:1, 0.32:1, 0.44:1, and 0.56:1, respectively.

Topography Analysis. Dispersion of clay in deionized water was analyzed by a commercial Nanoscope IIIa Multi-Mode AFM (Veeco Instruments, CA) in typing mode. The topographies were obtained at the scan size of 2 μm (data collection at 512 × 512 pixels) and the scan frequency of 1 Hz using a silicon nitride cantilever. The samples were prepared by a solution coating technique on a single crystal silicon plate. The concentration of clay in suspension used here is about 15 μg/ml. Quantitative determination of geometries of the dispersed clay and their distribution were performed by image analysis of AFM height topographies using Nanoscope V5.12 software. The morphology of the highly hydrated CMCs was analyzed by Nikon TE-2000U inverted optical microscope with ×40 objective lens.

Thermogravimetric Analysis. TG analysis was employed to quantitatively determine the real adsorbed content of chitosan in CMCs. Prior to the measurement, CMCs slurries prepared from different initial weight ratios were dried in a vacuum oven at 50 °C for 24 h and ground to powder. With sample weights of 10 mg, TG traces were then measured by a thermal analysis system (TA, U.S.A.) in the temperature range of 300∼1200 K under an air atmosphere. The adsorbed chitosan contents in the considered CMCs were approximately calculated from the weight loss of the samples at 500∼800 K according to the previous work reported by M. Darder et al.[28] To remove the effect of water, the real contents of chitosan in the measured samples were calculated as

$$m = \frac{\varphi_{CS}}{1 - \varphi_w} \times 100\% \quad (1)$$

Here, ϕ_{CS} and ϕ_w are the weight losses caused by chitosan and water, respectively.

Rheological Analysis. Oscillatory shear measurements of the highly hydrated CMCs slurries were performed on a strain-controlled rheometer (ARES, TA Instruments, New Castle, U.S.A.). Measurements were carried out using parallel plate geometry with 25 mm diameter and 1 mm gap at 25 °C. Prior to measurement, the samples were loaded onto the plate and left for 20 min to relax the stresses and obtain thermal equilibrium. Strain sweeps ranging from 0 to 100% were carried out to determine the proper conditions for dynamic measurements. Dynamic frequency sweep experiments measuring the complex viscosity (η^*), storage modulus (G') and loss modulus (G'') were performed as functions of angular frequency (ω) ranging from 0.1 to 100 rad/s. A fixed strain of 0.5% was used to ensure that measurements were taken well within the linear viscoelastic region. Steady-state shear measurements for CMCs slurries were performed over the shear rate range of 0.1∼100 s^{-1}. The experimental protocols employed for these measurements are virtually the same as those for the oscillatory shear measurements. Furthermore, to explore mechanical stability and recovery of CMCs, the samples were first loaded and presheared under the shear rates of 0.1, 1, 10, 40, 50, and 100 s^{-1} for 300 s. Then, dynamic time sweep with an angular frequency of 1 rad/s and a strain of 0.5% was applied immediately to record the evolution of G' and G'' within the testing time of 1000 s. As a contrast, the same dynamic time sweep was also performed for the same samples without suffering to the preshearing treatment. However, rheological measurements for pure exfoliated clay were not successfully performed here due to a failure to obtain clay slurry with the same water content from its suspension. It would not be the problem for us to make a comparison among the rheological properties of CMCs with different adsorbed chitosan content. For all of the experiments, a small amount of low-viscosity silicon oil was coated around the edge of the sample to prevent water evaporation. The effect of the silicon oil on the overall rheological behavior is negligible.

Results and Discussion

Adsorption of Chitosan and Its Effect on the Microstructure of CMCs at Highly Hydrated State. Figure 1A,B shows the height and phase images of the pre-exfoliated clay used here. Though a few multilayered particles can still be observed from the images, most of the clay particles were successfully exfoliated to single or few-layered clay with the average thickness of about 3 nm, as indicated by the section analysis result (Figure 1C). By the addition of chitosan, the obtained CMCs from different initial weight ratios are shown in Figure 1D. All of them exhibited an off-white slurry-like state. Table 1 presents the adsorbed content of chitosan in these CMCs. m approximately undergoes an increase from 2.1 to 8.7% with the increase of s. However, the increasing amplitude of m becomes somewhat slight when $s > 0.16$:1.

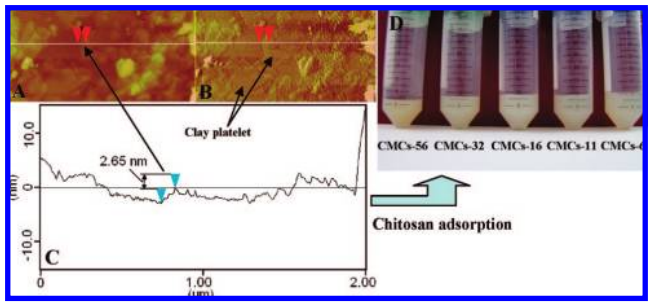

Figure 1. AFM height (A) and phase (B) images of the pre-exfoliated clay in distilled water. (C) Section analysis of the AFM height image. (D) Picture of the prepared CMCs.

TABLE 1: The Adsorbed Content of Chitosan in the Studied CMCs

samples	initial weight ratios ($s = W_{chitosan}/W_{clay}$)	adsorbed content of chitosan $m = (\phi_{CS})/(1 - \phi_w) \times 100\%$
CMCs-6	0.06:1	2.1
CMCs-11	0.11:1	4.7
CMCs-16	0.16:1	6.3
CMCs-22	0.22:1	6.9
CMCs-27	0.27:1	7.4
CMCs-32	0.32:1	8.1
CMCs-44	0.44:1	8.5
CMCs-56	0.56:1	8.7

Since rheological properties of materials are mainly determined by its time-dependence microstructure, microstructure of CMCs at a highly hydrated state was therefore studied by optical microscopy and the results are presented in Figure 2. CMCs-6 and CMCs-11 (Figure 2A,B) exhibit a relatively smooth and continuous structure, while CMCs-16, CMCs-22, CMCs-32, and CMCs-56 possess a networklike structure (Figure 2C,F). The networklike structure of CMCs with $m \geq 6.3\%$ becomes more obvious with the increase of the adsorbed chitosan content. This striking evolution in the microstructure of CMCs from smooth to networklike is due to the increase of the absorbed chitosan content on the clay surface. Considering the chitosan/clay weight ratios, smooth structure of CMCs-6 and CMCs-11 arises from the higher content of the clay platelets, which possess the major phase in this case. On the other side, at higher chitosan/clay ratios, most of the clay platelets are likely wrapped by chitosan chains. The interparticle interaction among

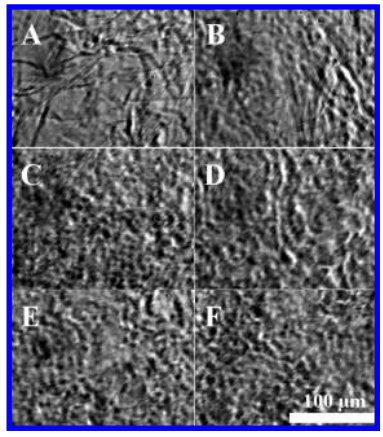

Figure 2. Optical microscopy images of CMCs-6 (A), CMCs-11 (B), CMCs-16 (C), CMCs-22 (D), CMCs-32 (E), and CMCs-56 (F) at highly hydrated state.

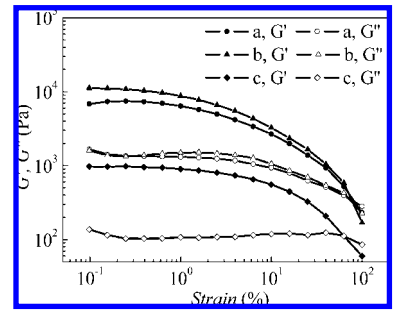

Figure 3. The storage modulus (G') and loss modulus (G'') of CMCs-6 (a), CMCs-16 (b), and CMCs-56 (c) as a function of the applied strain.

single CMCs particles is therefore enhanced through the interaction between those adsorbed chitosan chains, which lead to the formation of the networklike structure. Similar adsorption behavior has been well disclosed by adsorption isotherm study in CCN. Free chitosan chains are reasonable to exist in CMCs due to hydrogen bonding interaction between amino and hydroxyl groups on chitosan chain.[28]

Dynamic Rheological Properties of CMCs at Highly Hydrated State. Figure 3 presents the applied strain (γ) dependence of G' and G'' at the angular frequency of 2 rad/s. For simplicity, we only show the data from the samples of CMCs-6, CMCs-16, and CMCs-56. Payne effect, referring to the strain-dependence of the dynamic viscoelastic properties of filled polymers in the amorphous state, is observed in CMCs. In comparison with the strain-hardening behavior of end-tethered polymer nanocomposites, [41] CMCs here exhibit a strain-softening response at most of the applied strain range. Moreover, the strain-dependence of both G' and G'' is susceptible to m. As to G', a continuous and monotonous decrease with the increase of the applied strain is observed for both CMCs-6 and CMCs-16 at $\gamma > 1\%$. This strong strain-dependence of G' becomes somewhat less for CMCs-56 at lower shear strain. It is striking to observe that G'' of CMCs-56 shows a wider linear regime at the strain range of $0.25\% < \gamma < 40\%$ compared to that of CMCs-6 and CMCs-16. This extension in the linear regime implies that CMCs with higher m are more stable against the external strain. According to the results disclosed by optical microscopy, this phenomenon could arise due to the formation of the strong networklike structure at higher m. However, no obvious difference is observed between G'' for CMCs-6 and CMCs-16 in this regime. With a further increase of the applied strain, crossovers appear at the applied strain $\gamma > 60\%$ for all of the samples, indicating a transition from solidlike behavior to liquidlike behavior of CMCs. Obvious dependence of the crossovers on m is not observed for the samples considered here.

Angular frequency (ω) dependence of G' and G'' for CMCs over the frequency range of 0.1 to 100 rad/s is presented in Figure 4A,B, respectively. The strain amplitude is fixed at 0.5%, which is within the linear viscoelastic regime of CMCs. G' is higher than G'' over the entire range of the applied frequency for all of the studied CMCs. This fact indicates that the considered CMCs have a predominately elastic rheological response over the entire frequency range. No liquidlike to solidlike transition, which usually takes place at a certain critical content of clay in synthetic polymer-based nanocomposite melts, is observed at low frequency region for all of CMCs.[42−44] In Figure 4A, G' is nearly independent to the applied frequency in the region of $\omega > 50$ rad/s. The resulting modulus in the plateau is a combination of chitosan chains and the clay platelets. To further determine the effect of the adsorbed chitosan content

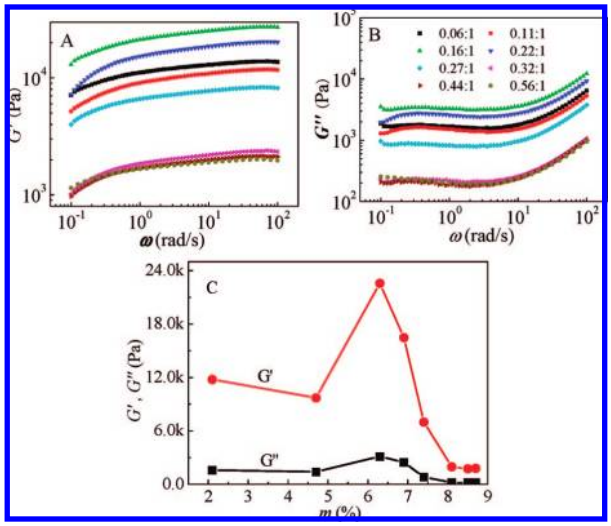

Figure 4. G' (A) and G'' (B) of CMCs as a function of angular frequency at $\gamma = 0.5\%$; (C) G' and G'' as functions of the adsorbed chitosan content at $\omega = 2$ rad/s and $\gamma = 0.5\%$.

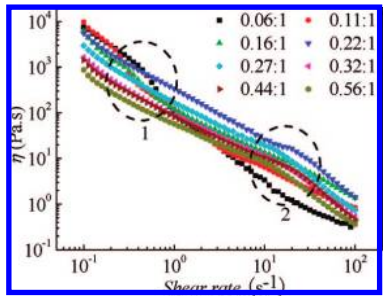

Figure 5. Shear viscosity (η) as a function of shear rate (0.1∼100 s^{-1}) for CMCs with s ranging from 0.06:1 to 0.56:1.

on G' and G'', the values of both G' and G'' obtained at $\omega = 2$ rad/s and $\gamma = 0.5\%$ are presented in Figure 4C as a function of m. One of the important reasons to choose these conditions for studying G' and G'' is that this lower frequency will not greatly change the structure of CMCs as compared to its original state. On the other hand, this frequency is so well matched that we were able to determine the linear viscoelasticity domain. Interestingly, with the increase of m, CMCs-16 shows the highest values of $G' \sim 22.6$ kPa and $G'' \sim 3.1$ kPa, which are largely higher than that of the other CMCs. Moreover, both G' and G'' of CMCs from $m \geq 7.4\%$ are lower than those of CMCs from $m < 7.4\%$. And a low modulus plateau of CMCs appears at $m > 7.4\%$. These results indicate that both G' and G'' show strong dependence on the adsorbed content of chitosan. In terms of the chitosan/clay weight ratios, the different contribution between the clay platelets and chitosan to the modulus of CMCs may responsible for this dependence. At low chitosan content, clay platelets acting as the major phase contributes the higher elastic part of CMCs. At high chitosan level, the clay platelets are totally wrapped by chitosan and the free chitosan chain left contributes more to the viscous part of the mixture. However, at a certain value of the chitosan/clay ratio (CMCs-16), the highest values of G' and G'' could arise from the formation of the continuous network. In such case, both clay and chitosan possess the best synergistic effect to the modulus of CMCs.

Steady-Shear Rheological Properties of CMCs at Highly Hydrated State. Shear viscosity (η) as a function of the applied shear rate ($\dot{\gamma}$) is presented in Figure 5. The shear viscosity of CMCs shows no Newtonian plateau but a quite complicated nonlinear decrease with the increase of the shear rate. Two

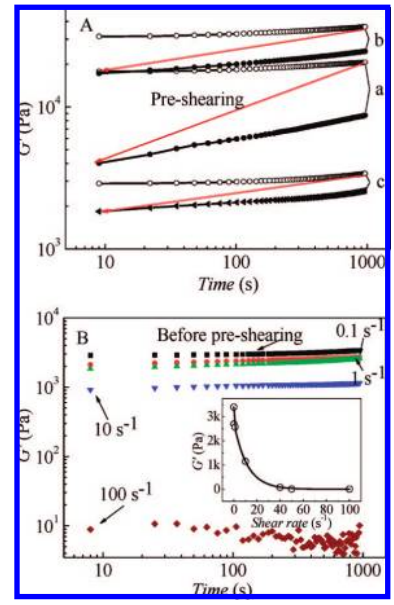

Figure 6. (A) Time dependence of G'_{After} for CMCs-6 (a), CMCs-16 (b), and CMCs-56 (c) after presheared at 1 s^{-1} for 300 s, respectively ((○) before shearing, (●) after shearing). (B) Time dependence of G'_{After} for CMCs-56 after presheared at the shear rates of 0.1, 1, 10, and 100 s^{-1} for 300 s, respectively. The inserted picture shows a relation between the applied shear rate and the values of G'_{After} at the end of each recovery test.

special transitions of η at the shear rate of about $0.2 < 0.2 < \dot{\gamma} < 0.5$ s^{-1} (region 1) and $10 < \dot{\gamma} < 40$ $s^{-1} < 40$ s^{-1} (region 2) are observed for the tested CMCs during the shearing process. The transition in region 1 exhibits a sharp drop of η while that in region 2 shows a small peak value of η. Strikingly, these transition behaviors of CMCs have a close dependence on the absorbed chitosan content. Compared to the two-transition characteristic of CMCs-11 and CMCs-16, there is only one transition for CMCs-6 in region 1 and only one transition for the other CMCs prepared from $s > 0.16{:}1$ in region 2. Moreover, in region 1, both the onset shear rate for the transition and the dropping amplitude in η of CMCs-11 and CMCs-16 is lower than that of CMCs-6. No obvious m dependence of the onset shear rate is observed for the transition in region 2. It is important to point out that, this rheological behavior is quite different from that of clay suspensions and chitosan aqueous solution. Clay suspensions with low clay concentration (1 wt %) were observed to exhibit a nearly linear shear-thinning behavior at the applied shear rate of 10^{-3}∼100 s^{-1} while chitosan dissolved in acetic acid/sodium acetate aqueous solution showed a Newtonian behavior at the shear rate range of 1∼100 s^{-1}.[45−47] The reasons to cause the above unique transitions will, however, be further clarified in the following section.

Effect of Chitosan on Mechanical Stability and Thixotropic Behavior of CMCs at Highly Hydrated State. To explain the above unique rheological properties of CMCs, the mechanical stability of CMCs was further investigated according to the decrease amplitude in the modulus of CMCs after suffered to a preshearing treatment at a certain shear rate. Changes in G' of CMCs-6, CMCs-16, and CMCs-56 before and after underwent a preshearing at $(\dot{\gamma}) = 1$ s^{-1} for 300 s are depicted in Figure 6A as a function of the recovery time. Compared to the storage modulus before preshearing (G'_{Before}), a large decrease in the modulus after preshearing (G'_{After}) is observed for all of the tested CMCs. This decrease in G' is due to the disorganization in the interparticle-connected microstructure of CMCs and orientation of CMC particles. For a more quantitative

illustration of the changes, the decrease amplitudes ($\Delta G'$) of the storage modulus before and after preshearing were calculated as the following

$$\Delta G' = \frac{G'_{\text{Before}} - G'_{\text{After}}}{G'_{\text{Before}}} \times 100\% \quad (2)$$

The maximum decrease amplitude of the storage modulus after suffered to the preshearing treatment is up to 77.4, 45.2, and 36.4% for CMCs-6, CMCs-16, and CMCs-56, respectively. It is therefore clear that the mechanical stability of CMCs is strengthened with the increase of the adsorbed chitosan content. Among those considered CMCs, CMCs-6 composed of the clay platelets as the major phase is the most affected system to the preshearing treatment as a result of the strong disorganization of the clay platelets. CMCs-56 is less affected by preshearing due to its lower elastic component and continuous network structure. CMCs-16 then can be logically characterized by an intermediate disorganization compared to the two extreme systems.

Furthermore, the recovery of CMCs at rest after the steady shear can be considered a fundamental thixotropic process. Monotonic increase of complex viscosity or modulus with the increase of recovery time has been observed in clay aqueous suspensions.[48] Typical thixotropic behavior of clay-water suspensions, which possess a time-dependent process, is usually associated with restoration and destruction of the structure of clay platelets.[49−52] In Figure 6A, continuous increase of G'_{After} for all of the considered CMCs within the time scale of measurement provides a direct proof for the thixotropic behavior of CMCs. The recovery amplitude of G'_{After} within the testing time is closely related to the adsorbed content of chitosan. It implies that the adsorbed content of chitosan has the ability to affect the restoring capability of CMCs. Moreover, a power law

$$G'_{\text{After}} \sim t^n \quad (3)$$

characterizing the kinetics of the thixotropic recovery of clay suspensions is applied to describe the linear relationship between log G'_{After} and log t in Figure 6A. Single exponent is valid over the time scale from 10 to 1000 s. The exponent n can be determined directly from the fitting slopes of the experimental curves of log G'_{After} versus log t. The determined values of n are 0.165, 0.082, and 0.072 for CMCs-6, CMCs-16, and CMCs-56, respectively. The results indicate that the time scale for CMCs to reorganize is largely prolonged with the increase of m. However, $n = 0.165$ for CMCs-6 is quite close to $n = 0.158$ observed in sodium montmorillonite aqueous suspensions.[48] Low chitosan content shows no obvious effect on the thixotropic nature of the clay platelets. It is worthy noting that, G'_{After} is still lower than G'_{Before} and no equilibrium is reached within the testing time.

Figure 6B presented are the recovery curves of G'_{After} for CMCs-56 obtained at the preshear rate of $(\dot{\gamma}) = 0.1$, 1, 10, and 100 s^{-1} (The curves from $(\dot{\gamma}) = 40$ and 50 s^{-1} are not shown here). It is quite clear that G'_{After} of CMCs-56 shows strong dependence on the applied steady shear. For a further description, G'_{After} values of CMCs-56 from the end of each recovery time are plotted as a function of the applied preshear rates. The result clarifies that G'_{After} decreases first with the increase of the applied shear rate and then reaches a plateau when $(\dot{\gamma})$ exceeds about 40 s^{-1}. In the plateau regime, the microstructure of CMCs-56 is almost fully disorganized by the strong steady shear, which causes more viscouslike of CMCs-56. Furthermore, the values of the exponent n were calculated as 0.054, 0.072, 0.043, and −0.157 for the shear rate of 0.1, 1, 10, and 100 s^{-1},

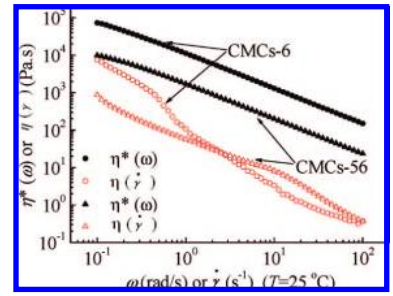

Figure 7. Test of Cox−Merz rule on the rheological behavior of CMCs-6 and CMCs-56.

respectively. These results indicate that the restoration of CMCs is strongly related to preshearing history. The negative value of n obtained at $(\dot{\gamma}) = 100$ s^{-1} suggests a full lack of restoration in the microstructure of CMCs within the time scale of measurement. Similar dependence of thixotropic flow on steady shear has also been reported in clay-water suspensions. [49]

Combined with the result from optical microscopy, it is therefore reasonable to explain the unique transitions of CMCs (Figure 5) according to the mechanical stability and thixotropic behavior of CMCs. For CMCs-6, sharp drop of η in region 1 is due to the synergistic effect of the orientation of CMCs particles and the sudden rupture of their weak interparticle-connected microstructure formed through some weak interactions such as Van der Waal force. For the CMCs with $m > 6.3\%$, the situation is quite different due to the formation of strong networklike structure that greatly strengthens the ability of CMCs to resist the external stress. This strong networklike structure only can be broken when the applied shear stress exceeds its yield point. In such a case, region 2 mainly stems from the full deformation of the networklike structure of CMS at its yield point. The lack of the sharp drop of the shear viscosity in region 1 is due to the partial deformation and orientation of the network-like structure at low shear rate. However, as the intermediate of these two extreme cases, CMCs-16 is logically characterized by these two transitions due to the coexistence of both the networklike structure and some weak particle-interconnected structure.

Test of Cox−Merz Rule on the Rheological Behavior of CMs at Highly Hydrated State. The ability of CMCs to alter their mesoscale structure and orient their basic particles under shear flow is further analyzed by employing empirical Cox−Merz rule. The analysis results of CMCs-6 and CMCs-56 are demonstrated in Figure 7. The Cox−Merz rule states that

$$\eta^*(\omega) = \eta(\dot{\gamma}) \text{ for } \omega = \dot{\gamma} \quad (4)$$

where, η^* (ω) and η $(\dot{\gamma})$ are frequency-dependence complex viscosity and shear viscosity, respectively. This relationship is generally acceptable for homopolymers and also some unfilled disordered liquid-like block copolymers. However, for the highly filled polymer matrix examined previously, $\eta^*(\omega)$ is always higher than η $(\dot{\gamma})$ with the magnitude of the difference increasing with the increase of silicate loading.[53,54] Figure 7 shows $\eta^*(\omega)$ always exceeds η $(\dot{\gamma})$ over the entire range of shear flow for both of CMCs-6 and CMCs-56, which indicates a failure to the Cox−Merz rule in this system. In accordance with those filled polymer systems, such a failure could arise due to some preferential orientation of the initial quiescent random arrangement of CMCs particles or their tactoids under a steady shear. Interestingly, the difference $(\Delta\eta)$ between $\eta^*(\omega)$ and η $(\dot{\gamma})$ shows a strong dependence on m. There is a rapid increase in $\Delta\eta$ with the increase of the shear rate or angular frequency for

CMCs-6, whereas a much slighter change is observed for that of CMCs-56. This result clearly demonstrates that the orientation of CMCs particles with lower m is more sensitive to the shear flow than that of CMCs with higher m. It agrees well with the result described in Figure 6A. The larger $\Delta\eta$ of CMCs-6 at higher shear rate may arise from the substantial alignment of CMCs particles.

Conclusion

As disclosed by optical microscopy, the microstructure of the highly hydrated CMCs possessed a remarkable evolution from relatively smooth to network-like structure with the increase of m. Rheological results indicated that all of the considered CMCs showed an elastic rheological response at $\gamma < 60\%$ while a solidlike to liquidlike transition occurred at $\gamma > 60\%$. With the highest moduli of CMCs-16 and the most extensively linear stress−strain region of CMCs-56, both moduli and stress−strain behavior of CMCs were closely related to the adsorbed chitosan content. Moreover, shear viscosity of CMCs showed a nonlinear decrease over the entire range of the applied shear rate, indicating a shear-thinning behavior. Two unique transitions in the shear viscosity including a small peak region around at $10 < (\dot{\gamma}) < 40\ s^{-1}$ and a sharp drop region around at $0.2 < (\dot{\gamma}) < 0.5\ s^{-1}$, were observed depending on m. Further, thixotropic behavior was observed in CMCs systems. Fitting of the exponent n indicated that the CMCs with lower m or with preshearing history from lower shear rate showed a stronger restoration capability within the testing time. The mechanical stability of CMCs was greatly enhanced by the adsorbed chitosan due to the formation of networklike structure at higher m. These differences in the mechanical stability of CMCs were therefore considered as the main reason to result in the strong m-dependence of the unique transitions and stress−strain behavior. The sharp drop region for CMCs with $m \leq 6.3\%$ was attributed here to the synergistic effect of the orientation of CMC particles and the sudden rupture of their weak interconnected-microstructure, while the small peak region for CMCs with $m > 2.1\%$ could arise due to the complete deformation of the strong networklike microstructure at its yield point. Failure to follow the Cox−Merz rule of CMCs further implied that shear-thinning in this system was closely related to some preferential orientation of the initial quiescent random arrangement of CMCs particles or their tactoids under the shear flow.

Acknowledgment. We thank Dr. Jozef Kokini for the use of rheology instruments. This work was supported by National Research Initiative Grant 2006-35503-17568 from the USDA Cooperative State Research, Education, and Extension Service Program on Improving Food Quality and Value.

References and Notes

(1) Giannelis, E. P. *Adv. Mater.* **1996**, *8*, 29–35.
(2) Suter, J. L.; Coveney, P. V.; Greenwell, H. C.; Thyveetil, M.-A. *J. Phys. Chem. C* **2007**, *111*, 8248–8259.
(3) Messersmith, P. B.; Giannelis, E. P. *Chem. Mater.* **1993**, *5*, 1064.
(4) Okamotoa, M.; Moritaa, S.; Taguchia, H.; Kima, Y. H.; Kotakaa, T.; Tateyamab, H. *Polymer* **2000**, *41*, 3887–3890.
(5) Chasteka, T. T.; Steina, A.; Macosko, C. *Polymer* **2005**, *46*, 4431–4439.
(6) Vaia, R. A.; Ishii, H.; Giannelis, E. P. *Chem. Mater.* **1993**, *5*, 1694.
(7) Ogata, N.; Jimenez, G.; Kawai, H.; Ogihara, T. *J. Polym. Sci., Part B: Polym. Phys.* **1997**, *35*, 389.
(8) Pavlidou, S.; Papaspyrides, C. D. *Prog. Polym. Sci.* **2008**, *33*, 1119–1198.
(9) Geoffrey, M.; Bowers, David; Bish, L.; James Kirkpatrick, R. *J. Phys. Chem. C* **2008**, *112*, 6430–6438.
(10) Kornmann, X.; Lindberg, H.; Berglund, L. A. *Polymer* **2001**, *42*, 1303.
(11) Manias, E.; Touny, A.; Wu, L.; Strawhecker, K.; Lu, B.; Chung, T. C. *Chem. Mater.* **2001**, *13*, 3516.
(12) Jacobs, J. D.; Koerner, H.; Heinz, H.; Farmer, B. L.; Mirau, P.; Garrett, P. H.; Vaia, R. A. *J. Phys. Chem. B* **2006**, *110*, 20143–20157.
(13) Vaia, R. A.; Giannelis, E. P. *Macromolecules* **1997**, *30*, 8000.
(14) Zerda, A. S.; Lesser, A. J. *J. Polym. Sci., Part B: Polym. Phys.* **2001**, *39*, 1137.
(15) Kim, C. M.; Lee, D. H.; Hoffmann, B.; Kressler, J.; Stoppelmann, G. *Polymer* **2001**, *42*, 1095.
(16) Lagaly, G. *Phil. Trans. R. Soc. London, Sect. A* **1984**, *311*, 315–332.
(17) Bujdák, J.; Komadel, P. *J. Phys. Chem. B* **1997**, *101,44*, 9065–9068.
(18) Lee, S. Y.; Echo, W. J.; Kim, K. J.; Ahn, J. H.; Lee, M. *J. Colloid Interface Sci.* **2005**, *284*, 667–673.
(19) Park, S. J.; Seo, D. I.; Lee, J. R. *J. Colloid Interface Sci.* **2002**, *251*, 160–165.
(20) Sasai, R.; Itoh, H.; Shindachi, I.; Shichi, T.; Takagi, K. *Chem. Mater.* **2001**, *13*, 2012–2016.
(21) Chivrac, F.; Pollet, E.; Schmutz, M.; Avérous, L. *Biomacromolecules* **2008**, *9*, 896–900.
(22) Park, H.; Liang, X.; Mohanty, A. K.; Misra, M.; Drzal, L. T. *Macromolecules* **2004**, *37*, 9076–9082.
(23) Park, H.; Misra, M.; Drzal, L. T.; Mohanty, A. K. *Biomacromolecules* **2004**, *5*, 2281–2288.
(24) Günister, E.; Pestreli, D.; Ünlü, C. H.; Atıcı, O.; Güngör, N. *Carbohydr. Polym.* **2007**, *67*, 358–365.
(25) Darder, M.; Löpez-Blanco, Aranda, M. P.; Aznar, A. J.; Bravo, J.; Ruiz-Hitzky, E. *Chem. Mater.* **2006**, *18*, 1602–1610.
(26) Wang, S. F.; Chen, L.; Tong, Y, J. *J. Polym. Sci., Part A: Polym. Chem* **2006**, *44*, 686.
(27) Xu, Y.; Ren, X.; Hanna, M. A. *J. Appl. Polym. Sci.* **2006**, *99*, 1684–1691.
(28) Darder, M.; Colilla, M.; Ruiz-Hitzky, E. *Chem. Mater.* **2003**, *15*, 3774.
(29) Tang, C.; Xiang, L.; Su, J.; Wang, K.; Yang, C.; Zhang, Q.; Fu, Q. *J. Phys. Chem. B* **2008**, *112*, 3876–3881.
(30) Galgali, G.; Ramesh, C.; Lele, A. *Macromolecules* **2001**, *34*, 852–858.
(31) Hyun, Y. H.; Lim, S. T.; Choi, H. J.; Jhon, M. S. *Macromolecules* **2001**, *34*, 8084–8093.
(32) Gupta, V. K.; Krishnamoorti, R.; Chen, Z. R. *Macromolecules* **1996**, *29*, 875–884.
(33) Krishnamoorti, R.; Giannelis, E. P. *Macromolecules* **1997**, *30*, 4097–4102.
(34) Krishnamoorti, R.; Yurekli, K. *Curr. Opin. Colloid Interface Sci.* **2001**, *6*, 464–470.
(35) Han, C. D. *Multiphase Flow in Polymer Processing*: Academic Press: New York, 1981.
(36) Han, J. H.; Feng, D.; Choi-Feng, C.; Han, C. D. *Polymer* **1995**, *36*, 155.
(37) Lee, K.; Han, C. D. *Macromolecules* **2003**, *36*, 8796–8810.
(38) Agrawal, S. K.; Sanabria-DeLong, N.; Tew, G. N.; Bhatia, S. R *Langmuir* **2008**, *24*, 13148–13154.
(39) Haraguchi, K; Takehisa, T. *Adv. Mater.* **2002**, *14*, 1120.
(40) Haraguchi, K.; Takehisa, T.; Fan, S. *Macromolecules* **2002**, *35*, 10162.
(41) Krishnamoorti, R.; Giannelis, E. P. *Langmuir* **2001**, *17*, 1448–1452.
(42) Huang, W.; Han, C. D. *Macromolecules* **2006**, *39*, 257–267.
(43) Solomon, M. J.; Almusallam, A. S.; Seefeldt, K. F.; Somwangthanaroj, A.; Varadan, P. *Macromolecules* **2001**, *34*, 1864–1872.
(44) Gupta, R. K.; Pasanovic-Zujo, V.; Bhattacharya, S. N. *J. Non-Newtonian Fluid Mech.* **2005**, *128*, 116–125.
(45) Shalkevich, A.; Stradner, A.; Bhat, S. K.; Muller, F.; Schurtenberger, P. *Langmuir* **2007**, *23*, 3570–3580.
(46) Baravian, C.; Vantelon, D.; Thomas, F. *Langmuir* **2003**, *19*, 8109–8114.
(47) Desbrieres, J. *Polymer* **2004**, *45*, 3285–3295.
(48) Li, S.; Hou, W.; Sun, D.; Guo, P.; Jia, C. *Langmuir* **2003**, *19*, 3172–3177.
(49) Joye, D. D.; Poehlein, G. W. *Trans. Soc. Rheol.* **1971**, *15*, 51–61.
(50) Pignon, F.; Magnin, A.; Piau, J. *J. Rheol.* **1998**, *42*, 1349–1373.
(51) Pignon, F.; Magnin, A.; Piau, J. *J. Rheol.* **1996**, *40*, 573–587.
(52) Nakaishi, K.; Yasutomi, R. *Appl. Clay Sci.* **1994**, *9*, 71–79.
(53) Larson, R. *The Structure and Rheology of Complex Fluids*; Oxford University Press: New York, 1999.
(54) Ren, J.; Krishnamoorti, R. *Macromolecules* **2003**, *36*, 4443–4451.

JP8107304